Dynamic response of rigid wheels on deformable terrains

DYNAMIC RESPONSE OF RIGID WHEELS ON DEFORMABLE TERRAINS

Chrysostomos-Alexandros Bekakos #1[a], George Papazafeiropoulos #2[b], Dan J. O'Boy[a], Jan Prins[c]

[a] *Department of Aeronautical and Automotive Engineering, Loughborough University #1, c.bekakos@lboro.ac.uk*
[b] *National Technical University of Athens #2, gpapazafeiropoulos@yahoo.gr*
[c] *Jaguar Land Rover*

Abstract

Off-road vehicle performance, such as vehicle mobility, maneuverability, and traction performance is generally affected by the pneumatic tyre-off-road terrain interaction. Modelling of such cases is usually based on empirical and semi-empirical solutions, which have limited applicability in real situations due to their inherent weaknesses. In this study, numerical simulation of the dynamic mobility of a rigid wheel on a deformable terrain is performed through a series of transient nonlinear dynamic finite element analyses with the use of the finite element code ABAQUS (v. 6.13). The dynamic interaction of a rigid wheel with the underlying soil during off-road vehicle travel is simulated. The effects of the vertical load carried by the wheel, the tread pattern, the longitudinal and lateral tread parameters, and the slip ratio of the wheel on the wheel performance are investigated and useful results are extracted. The numerical results reveal that the effects of the tread pattern, particularly tread depth and the terrain constitutive properties, such as soil cohesion can be of high importance for the general wheel response.

Keywords: Tyre-Soil Interaction, Rigid wheels, Drucker-Prager

1. Introduction

The ability of tracked and wheeled vehicles to traverse certain types of deformable soils is of main importance. In order to properly understand and accurately model the behaviour of a rolling wheel on a soft terrain the dynamic interaction between the wheel and the soil has to be taken into account. Due to the large number of parameters controlling this phenomenon, assumptions have to be made in order to obtain computationally reasonable results. Therefore, simplified models have been developed in the past to simulate the rolling response of a wheel interacting with a deformable terrain. The dynamic nature of the wheel–soil interaction combined with the kinematics of the moving vehicle which involve large displacements makes the problem complicated, the solution of which necessitates the use of advanced numerical methods, like the finite element method. The study of the wheel soil interaction gives more accurate results which lead to reliable and economical design of the vehicles moving on deformable terrains.

In this study the indentation and rolling behaviour of a rigid wheel is considered. The steady state response of the wheel-soil system subjected to quasi-static loads will be estimated. Two soil failure criteria are implemented to account for the soils bearing capacity for large deformations. The cases of laterally and longitudinally treaded wheel are examined, and their results are compared to those of the treadless wheel. Useful conclusions have been drawn from the results of this study. However, it is observed that the wheel-soil interaction phenomenon is complicated and further research needs to be made to identify the most important parameters and the way they influence the response of the wheel-soil system.

2. Literature Review

The response of a rolling wheel on a deformable soil can be described by a pressure – sinkage relationship and a shear stress – normal pressure relationship. The methods developed for modeling of a vehicle's mobility can be classified into three categories: empirical (semi-analytical) methods, analytical methods and numerical methods.

2.1 Empirical Methods (or Semi-Analytical methods)

In order to predict motion resistance of a rigid wheel on soil, Bekker (1956) assumed that the radial terrain reaction at all points on the wheel – soil contact surface is equal to that under a plate penetrated to the same depth according to the relation:

$$\sigma_n(\theta) = \left(\frac{k_c}{b} + k_\varphi\right) z^n(\theta) \qquad 1$$

The various parameters (k_c, k_φ, n) can be obtained by the results of plate penetration tests, however, these are non-invariant parameters which are highly dependent on the size and the dimensions of the plate and the soil specimen. It is noted that k_φ and k_c have dimensions dependent on the value of n, also a shortcoming of the model. The angle θ is shown in Fig. 1.

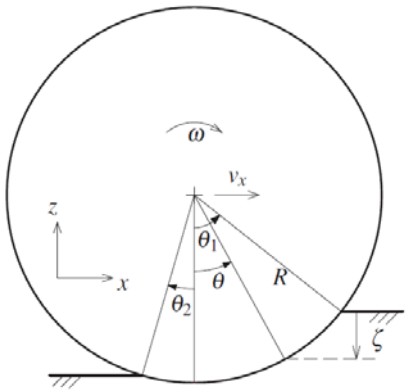

Fig. 1. *Rigid wheel in contact with soft soil.*

The shear stress-displacement relationship, proposed by Janosi & Hanamoto (1961) and obtained from shear tests, can be expressed for homogeneous soils as follows:

$$\tau(\theta) = \left(c + \sigma_n(\theta)\tan\varphi\right)\left[1 - e^{-j_d(\theta)/K_d}\right] \qquad 2$$

This equation is successfully applied for soils not exhibiting a hump in their shear stress – shear displacement diagrams, such as loose sand, saturated clay, dry fresh snow and most of the disturbed soils. Various relations for the shear displacement j_d have been proposed in the literature. For soils which are exhibiting a hump two distinct categories were identified by Wong & Preston-Thomas (1983) and respective relations have been proposed.

Wong and Reece (1967a) proposed Eq. 3 for a driven wheel, which is the most widely adopted:

$$j_d(\theta) = R\left[(\theta_1 - \theta) - (1 - i_s)(\sin\theta_1 - \sin\theta)\right] \qquad 3$$

Where i_s is the wheel slip ratio, defined as:

$$i_s = 1 - \frac{v_x}{R\omega} \tag{4}$$

Equation 3 is obtained by integrating the slip velocity in the contact region from the initial point of contact with the soil, identified by the angle θ_1, to the current angle θ and by assuming a constant slip ratio.

Wong & Reece (1967b) also studied the performance of towed rigid wheels. The normal stress distribution is calculated as:

$$\sigma_n(\theta) = \begin{cases} (k_1 + k_2 b)\left(\frac{R}{b}\right)^n (\cos\theta - \cos\theta_1)^n, \theta_t \le \theta < \theta_1 \\ (k_1 + k_2 b)\left(\frac{R}{b}\right)^n \left\{\cos\left[\theta_1 - \frac{\theta - \theta_2}{\theta_t - \theta_2}(\theta_1 - \theta_t)\right] - \cos\theta_1\right\}^n, \theta_2 \le \theta < \theta_t \end{cases} \tag{5}$$

Where k_1, k_2 and n are considered to be pressure-sinkage constants. Wong & Reece (1967b) used Eq. 2 for the shear stress- shear displacement relationship, where the shear displacement is taken from Eq. 3 for the rear region and from the following Eq. 6 for the front region:

$$j_d = R\left[(\theta_1 - \theta)\frac{(1 - i_s)(\sin\theta_1 - \sin\theta_t)}{\theta_1 - \theta_t} - (1 - i_s)(\sin\theta_1 - \sin\theta)\right] \tag{6}$$

Concluding the performance of rigid wheels on deformable soils depends largely on the soil properties. Three main categories of soils are described by Wong & Preston-Thomas (1983), according to their shear stress - shear displacement diagram. In the first category, by increasing the shear displacement the shear stress also increases up to a certain maximum and then continuously decreases. In the second category the shear stress increases up to a certain pick and then decreases up to a constant value where by further increasing the shear displacement no variation of the shear stress is occurring. The third category refers to soils for which eq. 2 is applied and respective equations for the first two categories have been produced.

The vast majority of the empirical relations presented in the literature are extensions and/or modifications of the aforementioned basic approaches. However, in this study only the most widely used are mentioned. When the normal and shear stress distributions around the wheel are known, the resultant soil reactions (motion resistance, traction force, resisting moment, terrain vertical reaction force, drawbar pull, etc.) can be calculated by appropriate integration of the stress distributions.

2.2 Analytical Methods

To provide a physical basis for the form of the equations, analytical methods were developed. These methods are correlating the normal pressure and vertical displacement with invariant parameters. Ageikin (1981) developed one of the first analytical relationships correlating the average ground pressure p with the sinkage z through soil bearing capacity factors. However, this equation is of limited applicability, mainly due to the fact that the normal stress under a plate contact area depends on the maximum pressure and not on the average ground pressure.

Lyasko (2010) proposed an analytical model with four basic invariant parameters, (soil cohesion c, internal friction angle φ, soil unit weight γ, and dynamic Young modulus E) which can be given or measured for any terrain by using classical soil mechanics or routine test methods through hand held instruments. The normal pressure is given as:

$$p = \frac{1}{\frac{D_1}{B_i} + \frac{D_2}{Ez}\omega b \xi} \tag{7}$$

where D_1, D_2, ω, ξ are dimensionless parameters.

Some difficulties exist with this method, such as the inability of accurately measuring soil characteristics like the hardpan depth (the thickness of the upper layer of the soil which can be deformed under loading).

Hambleton & Drescher (2008, 2009), presented a different approach and studied both the indentation and the rolling response of rigid wheels on deformable terrains. They proposed the so-called inclined force method and the inclined footing method. Limitations also exist within these methods, mainly for frictional soils, since they assume that the soil behaves as an elastic-perfectly plastic material and that the wheel-soil contact area can be considered equivalent to a flat rectangular surface with area determined purely by the vertical displacement into the soil.

Analytical equations relating the shear stress-normal pressure have been also developed; however they will not be presented here, since the three already mentioned semi-analytical methods are fitting to an acceptable degree of accuracy most of the experimental results available in the literature review.

2.3 Numerical Methods

With the increase in computing power, most of the researchers have focused on developing three dimensional models that can deal with complicated wheel-soil systems. Different numerical methods have been developed (e.g. the finite element method (FEM), the discrete element method (DEM), the smooth particle hydrodynamics method (SPH), etc). Within the first two methods, parts are described as an assemblage of elements, either interconnected at certain nodes (FEM) or as discrete elements (DEM). For the SPH method there is a centroid element which is being affected by the surrounding elements within a certain radius. Combining these methods is the best way to exclude their various assumptions and shortcomings, particularly these related to increased computational effort.

The tyre-soil interaction has been already studied by a number of researchers. Shoop (2001) used a nonlinear Drucker-Prager Cap Plasticity model which allows for the incorporation of the triaxial compression and triaxial tension of the soil material. An assumption generally accepted is that tyres with relatively high inflation pressure rolling on soft terrains behave virtually as rigid wheels. Chiroux et al. (2005) modeled the interaction of a rigid wheel with a deformable terrain using again the nonlinear Drucker-Prager Cap Plasticity model and observed that the soil tends to rebound after the passage of the wheel. This observation was also slightly noticed by the authors in the results of the current study.

Hambleton & Drescher (2008, 2009) studied the response of a rigid wheel while being indented and rolling on deformable soil respectively. The soil is modeled as an elastic-perfectly plastic material and the effects of varying wheel aspect ratio on the sinkage and required horizontal force are demonstrated. In Bekakos (2014) a rigid wheel with only longitudinal and only lateral tread patterns interacting with a nonlinear Drucker-Prager soil material is being studied. It was shown that larger shear stresses are developed in the case of lateral treads, in relation to the longitudinal treads.

3. Numerical Modeling

3.1 General

The indentation and the rolling response of a rigid wheel interacting with a deformable terrain are modeled numerically using the finite element code Abaqus 6.13. An explicit integration procedure was implemented by using Abaqus/Explicit, since it allows for a solution which is less computationally expensive and less susceptible to errors (e.g due to excessive element distortion, etc.), especially when adaptive meshing rules are used. Symmetry conditions were assumed about a plane normal to the road; thus only one half of the model was created. For the indentation model two steps were used; in the first step the gravity was applied at the soil, and in the second step a predefined sufficiently small velocity was applied on the wheel for a given time duration. Regarding the rolling wheel model again two steps were used, where in the first step the gravity was applied and in the second step a vertical force and a horizontal velocity were imposed at the center of the wheel in appropriate time instants, such that the wheel rotates with constant velocity under a constant vertical load over a given time period.

3.2 Geometry

The model is comprised of a 3D rigid wheel with diameter d and width b and a deformable road. The road was 3.0 m in length, 0.5 m in height and 1.0 m in width. Different aspect (i.e. wheel width to wheel diameter) ratios were set in the model. As a starting case, a wheel with b/d=0.3 was created. The road was partitioned appropriately, so that in the areas closer to the surface and to the rolling region the mesh was finer; the mesh was coarser in regions far from the

wheel. The wheel was located 0.74 m in front of the starting point of the soil so that sufficient space was left from the wheel contact patch for the development of stress and deformation. The inclusion of a fillet around the edges of the wheel was mandatory in order to avoid numerical instabilities caused by sharp edges on the circumference of the wheel. Rigid wheels with only lateral and only longitudinal tread patterns were considered. In the former case the lateral tread was added as an extra rigid part and by using a tie constraint, the elements of the tread were tied with the elements of the wheel. In the latter case the longitudinal treads were created by "cutting" region out of the initial rigid wheel. The configuration of the model used in the current paper is presented in Fig.2.

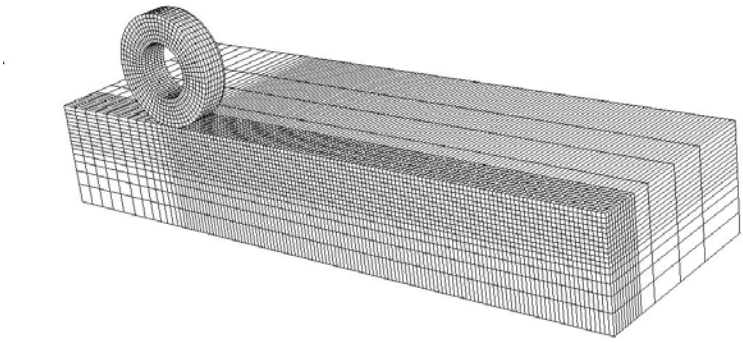

Fig. 2. *Reference configuration of the model used for the numerical simulations.*

3.3 Parameters

For the indentation process purely cohesive and purely frictional soils were studied, while for the rolling procedure and specifically for the frictional soils the cohesion was set sufficiently larger to avoid numerical instabilities of the analysis. For the indentation, the cohesive soils were defined with $\varphi=0^o$ and dimensionless cohesion $c/\gamma gd=1.25$ and for the frictional soil with a friction angle of $\varphi=45^o$ and dimensionless cohesion $c/\gamma gd=1.25 \times 10^{-2}$. For the rolling process and for the cohesive soils the soil parameters were identical to the indentation process while for the frictional/cohesive soils the friction angle was $\varphi=45^o$ and the dimensionless cohesion was set to $c/\gamma gd=0.25$. For the indentation process the wheel was predefined with a velocity boundary condition to move vertically until it reaches the maximum dimensionless sinkage $s/d=0.1$. For the rolling process, a constant vertical force was applied on the wheel, equal to $Q_v=1.9\gamma gbd^2$. The soil unit weight and the vertical force Qv were applied with a ramp amplitude over a period of $60d(\rho/E)^{1/2}$ and $180d(\rho/E)^{1/2}$ respectively, and the total duration of the second step was equal to $1180d(\rho/E)^{1/2}$. Concentrated mass equal to Qv/g, as well as rotary inertia were added to the wheel center. The rotary inertia was set to a nonzero number to avoid firstly numerical problems emerging from zero pivots. At the same time, the last was selected to be sufficiently small to avoid interference of the inertial behavior of the wheel to the steady state results.

3.4 Assumptions

The soil is considered to be homogeneous and the wheel was considered as rigid body through a rigid body constraint. The velocity of the wheel was kept steady during the rolling process and it was set to act instantaneously. Contact between the wheel and the road for the tangential direction was governed by the Coulomb friction rule with friction coefficient equal to 0.5 and for the normal direction hard contact was specified. The base and the outer sidewalls of the soil were fully constrained in all three translational degrees of freedom. Symmetric boundary conditions were applied on the inner side of the road so that the symmetry of the half model can be utilized. The rigid wheel was coupled with a reference point (RP) located at its center through a coupling constraint. The RP is set to have no lateral displacement, so that it can only move in the vertical and longitudinal directions.

3.5 Material models

The Mohr-Coulomb (MC) and the linear Drucker-Prager (DP) failure criteria were chosen to represent the plastic deformation of the soil. Equations that correlate the friction angle and the cohesion between these two failure criteria

already exist only for specific cases, e.g. triaxial compression or tension, plane stress/strain conditions, etc. However, in the rolling motion of a wheel, the problem becomes essentially three dimensional, in which case the various principal stresses are diverse and consequently there is not a unique way to match the one model to the other.

A novel relationship has been developed which can be used to approximately match the two constitutive models. The yield surface for DP is:

$$F_{DP} = \sqrt{\left(\sigma_1 - \sigma_2\right)^2 + \left(\sigma_2 - \sigma_3\right)^2 + \left(\sigma_3 - \sigma_1\right)^2} + \frac{1}{3}\left(\sigma_1 + \sigma_2 + \sigma_3\right)\tan\beta - d_{DP} \quad (8)$$

and the yield surface for MC is:

$$F_{MC} = \left(1 + \sin\varphi\right)\sigma_1 - \left(1 - \sin\varphi\right)\sigma_3 - 2c\cos\varphi \quad (9)$$

By setting equal the two normal vectors of the DP and MC yield surfaces at an arbitrary principal stress state, the following relations result:

$$\beta = \arctan\left(2\sin\varphi\right) \quad (10)$$

$$d_{DP} = 2c\cos\varphi \quad (11)$$

The two last equations were used to convert the MC parameters to DP parameters in ABAQUS and vice versa. The flow stress ratio in the DP model was set to unity which means that the yield stress in triaxial tension is equal to the yield stress in triaxial compression.

3.6 Mesh Adaptivity

During the modeling process of the indentation and the rolling procedure of the rigid wheel, high element distortion was observed on the soil, causing numerical errors and convergence instabilities. To avoid these issues the adaptive meshing (ALE) option offered in Abaqus/Explicit was utilized in the simulation. One remeshing sweep every 10 increments was performed, where the calculation of the new mesh is based on the priority of improving the aspect ratio of the elements. The ALE was set only on the region of the model where the fine mesh was located. Given that ALE cannot be implemented in a parallel processing mode, the size of the mesh was minimized, since otherwise high computational cost may occur. A mesh sensitivity study has been performed and the final mesh size was chosen such that the reduction of the element size in successive refinements gave an error of lower than 5%.

4. Results

4.1 Indentation

In the current paper the wheel indentation process is being modelled as a quasi-static procedure and the results are validated with numerical and experimental results from the literature. Results are being presented for two distinct soil categories; cohesive soils and frictional soils. Both the MC and DP failure criteria are being used and a comparison of their behavior is being presented.

Figure 3(a) illustrates a comparison between the MC and DP failure criteria for the indentation of a rigid wheel with aspect ratio b/d=0.3 on a cohesive soil. It is obvious that the numerical results associated to the DP criterion fit closely to the corresponding results associated to the MC criterion as well as the numerical results found in Hambleton & Drescher (2008). The dimensionless vertical force that is required for a specific sinkage of the wheel increases monotonically for s/d<0.1; however, the rate of increase gradually decreases as sinkage increases. This fact can be attributed to local soil failure occurring as the wheel displaces downwards.

In Fig. 3(b) the corresponding results for a frictional soil are being presented. In contrast to the cohesive soil, herein the MC failure criterion seems to overestimate the expected results. However, the DP criterion fits closely the results

from Hambleton & Drescher (2008). Additionally, in both Fig.3(a) and Fig.3 (b) it was observed that for small values of vertical displacements there is good agreement between the results of the two types of soils, while with further increase in the sinkage the DP criterion seems to be more reliable. For the frictional soil a non-associated flow was used ($\varphi \neq \psi$), since frictional models with associated flow were proved to be unstable. The vertical force varies in a quasi-linear way with sinkage in the case of frictional soil.

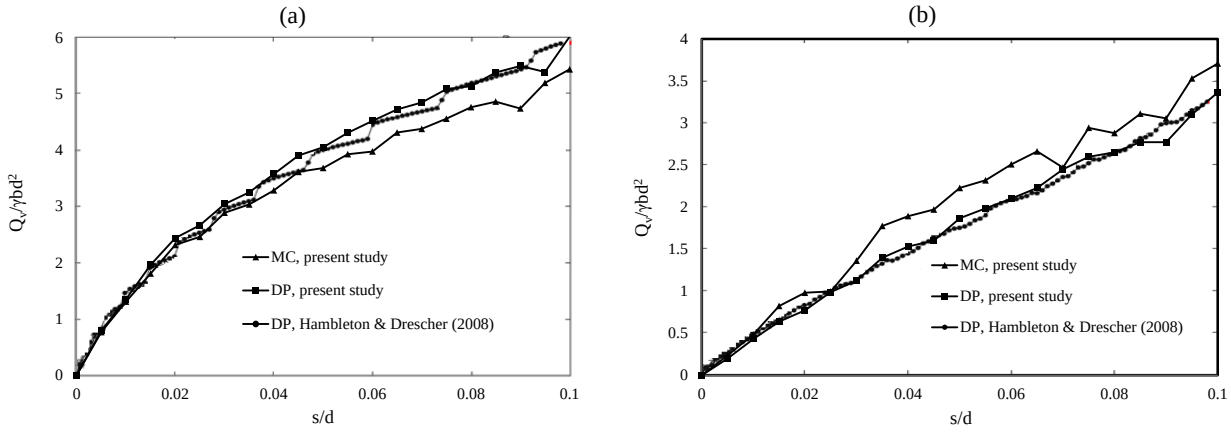

Fig. 3. *Dimensionless vertical load versus dimensionless sinkage for wheel with b/d=0.3 and (a) cohesive soil ($\varphi=0^o$, $\psi=0^o$ and $c/\gamma gd=1.25$), (b) frictional soil ($\varphi=45^o$, $\psi=0^o$ and $c/\gamma gd=1.25 \times 10^{-2}$).*

4.2 Rolling

The rolling process of a rigid wheel with and without tread patterns was studied. Initially a treadless wheel was developed and different aspect ratios (b/d) were examined. Typical aspect ratios for wheel are within the limits of $0.1 \leq b/d \leq 0.5$; however, in this study, aiming to highlight the various trends in the results, wheels with a maximum of b/d=1.0 have been considered. Similar to the indentation results, the results of the rolling motion were validated with numerical and experimental results from the literature review (Hambleton & Drescher, 2009). Once the treadless rolling rigid wheel model was validated the lateral and longitudinal treads were added.

Figure 4(a) illustrates the sinkage of a wheel with aspect ratio of s/d=0.3 rolling on a cohesive soil and carrying a vertical load equal to and $Q_v/\gamma bd^2=1.9$. It is observed that the sinkage after the imposition of the vertical force increases until it reaches a peak value, which occurs after the imposed vertical force has reached its maximum value. After this peak value, the sinkage decreases and eventually it stabilizes at a constant value, which is called the steady-state sinkage. Steady-state response is presented for a simulation time of roughly 10 sec. It has to be noted that the time period required for the wheel to attain its steady-state response is a function of its size (diameter) and the soil properties (density and elasticity modulus). Figure 4(b) shows the steady-state sinkage versus the applied vertical load at the wheel center. Several simulations with different vertical loads were required in order to obtain the curve shown in Fig.4(b). Good agreement is observed when the produced results are compared to numerical and experimental results from the literature (Hambleton & Drescher, 2009).

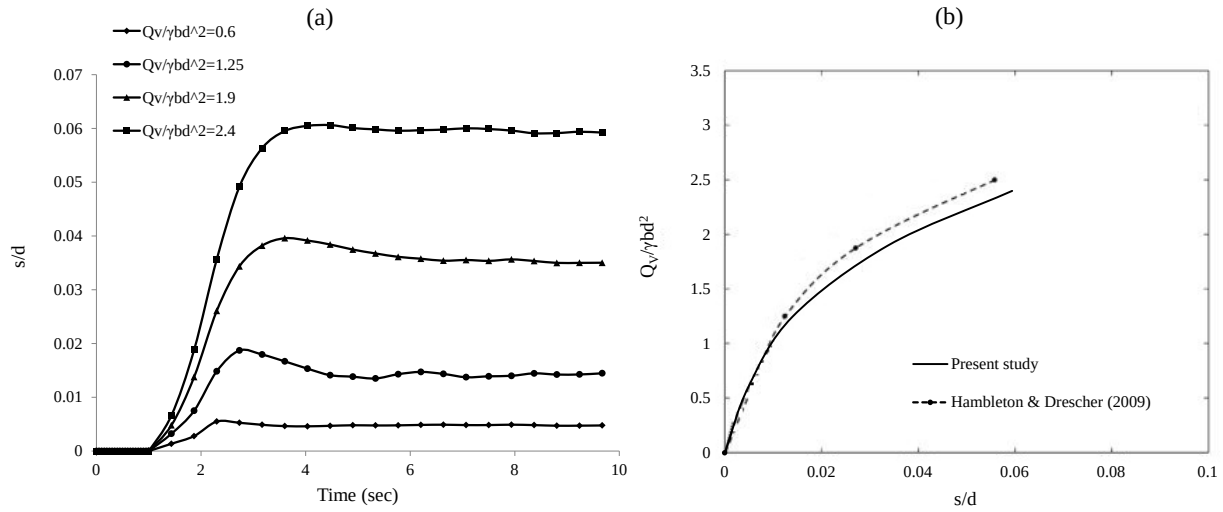

Fig. 4. *(a) Dimensionless sinkage versus time for wheel with b/d=0.3 ($\varphi=0^o$, $\psi=0^o$, $c/\gamma gd=1.25$) and various values of dimensionless vertical load ($Q_v/\gamma bd^2$), and (b) Dimensionless steady-state sinkage for a wheel with aspect ratio b/d=0.3 ($\varphi=0^o$, $\psi=0^o$ and $c/\gamma gd=1.25$).*

Different aspect ratios of a treadless wheel have been considered for both cohesive and frictional soils. The results for sinkage until steady state response are presented in Fig.5(a) and (b) respectively. It is clearly shown that by increasing the aspect ratio of the wheel and for the same amount of vertical load the transient as well as the steady state vertical displacement is decreasing. However, by increasing the aspect ratio the soil's accumulation in front of the wheel increases, causing an increase in the rolling resistance. This bulldozing effect has been noticed in almost all rolling models considered in the current study, a typical case of which is shown in Fig.6, where the deformed geometry of the soil after its interaction with the wheel is shown. In addition, in the cases involving the rolling wheel on frictional soils the cohesion was set to a larger value than that in the cases where wheel indentation was modeled, in order to avoid any numerical instabilities during the solution. Although both the MC and the DP failure criteria have been used for modeling the rolling wheel response, only the results corresponding to the DP failure criterion are presented here.

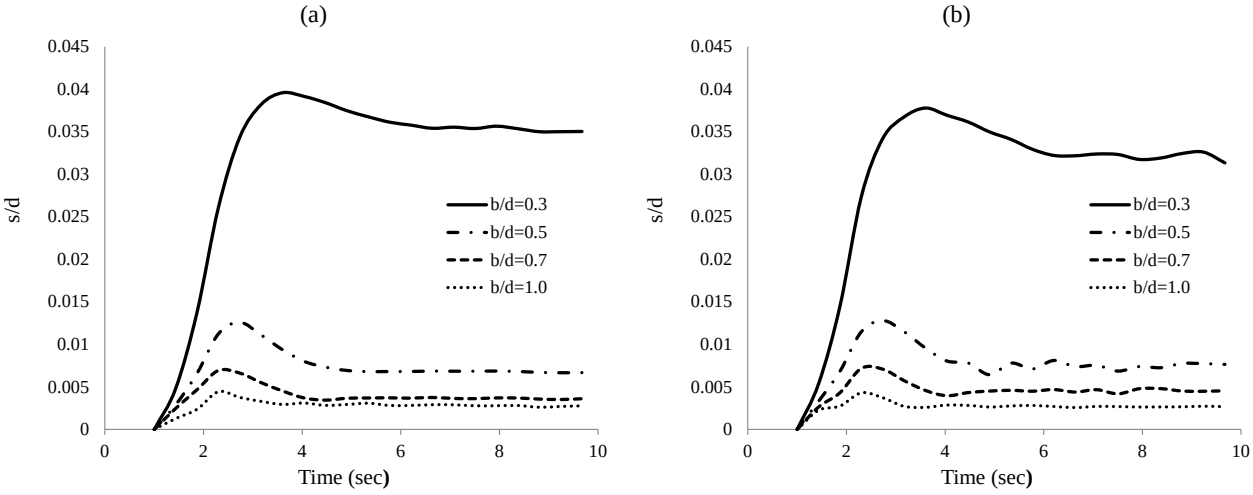

Fig. 5. *Dimensionless sinkage versus time for various aspect ratios of the wheel: (a) $\varphi=0^o$, $\psi=0^o$ and $c/\gamma gd=1.25$, $Q_v/\gamma bd^2=1.9$, (b) $\varphi=45^o$, $\psi=0^o$ and $c/\gamma gd=0.25$, $Q_v/\gamma bd^2=1.9$.*

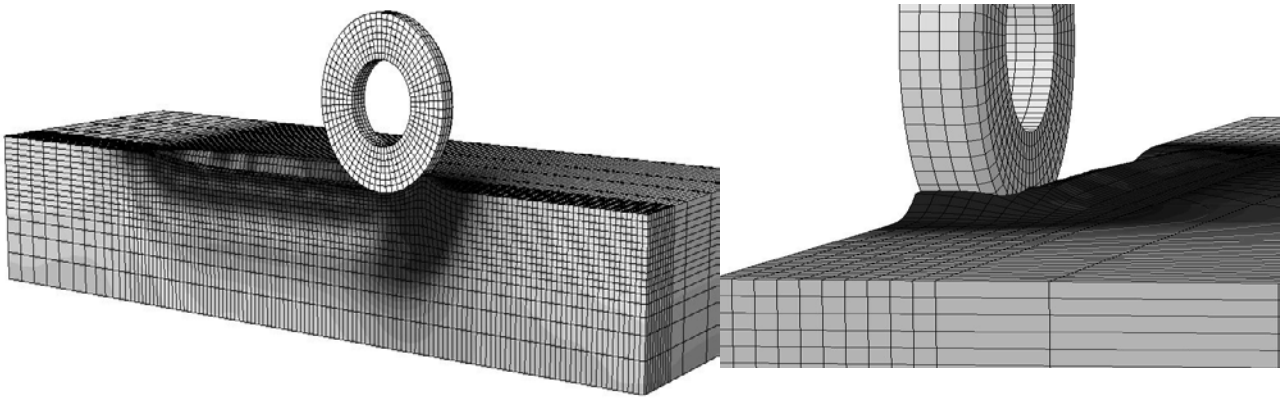

Fig. 6. *Wheel with b/d=0.3 ($\varphi=0^o$, $\psi=0^o$, $c/\gamma gd=1.25$, $Q_v/\gamma bd^2=2.4$), Left view: direction of travel from left to the right. Right view: front view of the wheel.*

The effect of the dilation angle on the rolling response of the treadless wheel is demonstrated. Various dilation angles for soil with non-associated flow were examined for a frictional soil and the steady-state results are presented in Fig. 7. Similar analyses have been performed by the authors for purely cohesive soils, but due to numerical instabilities associated with the failure models involved, the dilation angle cannot be much larger than the friction angle, so their results are not presented here. It is apparent in Fig. 7 that under constant vertical load and with increasing dilation angle the bearing capacity of the soil increases which leads to lower sinkage of the wheel into the soil. This fact has been already noted in the literature; for example Borst & Vermeer (1984) carried out finite element analyses for strip and circular footings on a material with $\varphi=40^o$ and dilation angle $\psi=20^o$ and $\psi=40^o$, where it was found that the analysis with higher angle of dilation showed a peak bearing capacity about 13% higher than that with the lower dilation angle.

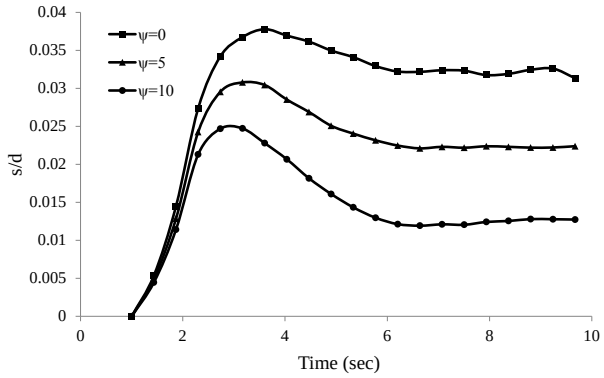

Fig. 7. *Dimensionless sinkage versus time for a rolling wheel with b/d=0.3, $\varphi=45^o$, $c/\gamma gd=0.25$, $Q_v/\gamma bd^2=1.9$ for various values of the soil dilation angle.*

Except for the treadless wheel, longitudinally and laterally treaded wheels were also considered in this study. An aspect ratio of b/d=0.5 was chosen for the treaded wheel. Initially, longitudinal tread patterns were created on the wheel and its rolling behavior on frictional and cohesive soils was examined. The longitudinal tread patterns are characterized by two quantities which have dimensions of length: (a) the depth of the tread, denoted by "e", and (b) the width of the tread contact area, denoted by "t". Therefore, a dimensionless longitudinal tread parameter can be defined by the ratio of the two aforementioned lengths, e/t. In Fig. 8 the values of dimensionless horizontal displacement (along the axis of wheel motion) and dimensionless horizontal force developed on the wheel for a frictional soil and two different tread depths are presented. For the given vertical load of $Q_v/\gamma bd^2=1.9$ the wheel with smaller ratio e/t requires higher horizontal force than the wheel with higher ratio e/t. This is caused mainly due to the fact that the longitudinal treads

with higher e/t ratio are not totally filled with soil, thus producing a resultant traction force which is mainly caused by the tread area which comes in contact with the underlying soil. On the other hand the longitudinal treads with smaller e/t ratio are filled with soil to a higher degree than in the former case, which results in higher traction at the wheel – soil contact area, since most of the contact patch interacts with the soil. By further increasing the vertical load the wheel with the larger e/t ratio requires even greater horizontal force to move. Hence, the optimum e/t ratio for a tyre depends mainly on the soil properties and the respective bearing capacity factors. It is clear that for different vertical loads the steady state response of the wheel varies accordingly.

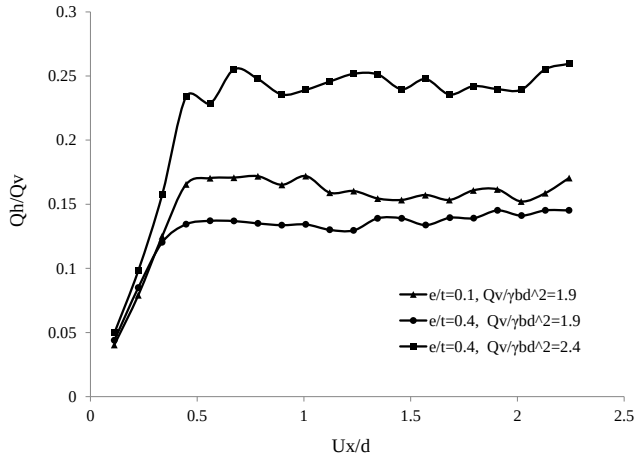

Fig. 8. *Ratio of required horizontal force to vertical load of rolling wheel with b/d=0.3 ($\varphi=45^o$, $c/\gamma gd=0.25$) for various combinations of longitudinal tread ratio e/t and dimensionless vertical load $Q_v/\gamma bd^2$.*

Finally, a laterally treaded rolling wheel was considered with aspect ratio b/d=0.5. The lateral treads were described in an analogous manner with the longitudinal treads, by two parameters: (a) the ratio of the tread height to the wheel diameter (e/d) and (b) the ratio of the tread contact area to the wheel diameter (t/d). The lateral treads were created on the wheel perimeter based on their epicentral angle, φ_d, which is the angle with vertex at the wheel center and corresponding to the circular arc of the tread. Figure 9 illustrates the results from a rigid rolling laterally treaded wheel. Several analyses have been conducted and the slip ratio was measured for each model. The slip ratio has already been defined in Eq.1, and relates the translational motion of the wheel to its respective rotational motion. In an ideal case in which no slip occurs between the wheel and the soil, the slip ratio is zero by definition. Each curve in Fig. 9 corresponds to a constant t/d ratio, and describes the variation of the mean value of the slip ratio with the e/d ratio. It is observed that for constant t/d ratio of the wheel, as the e/d ratio increases, the mean slip ratio decreases, and this is expected since for increasing e/d the lateral treads at the perimeter of the wheel control in a higher degree its overall rolling response. However, there is not any clear trend regarding the variation of t/d, for constant e/d, as it is observed that for the largest t/d ratio, the mean slip ratio remains in an intermediate range with respect to lower values of t/d.

.

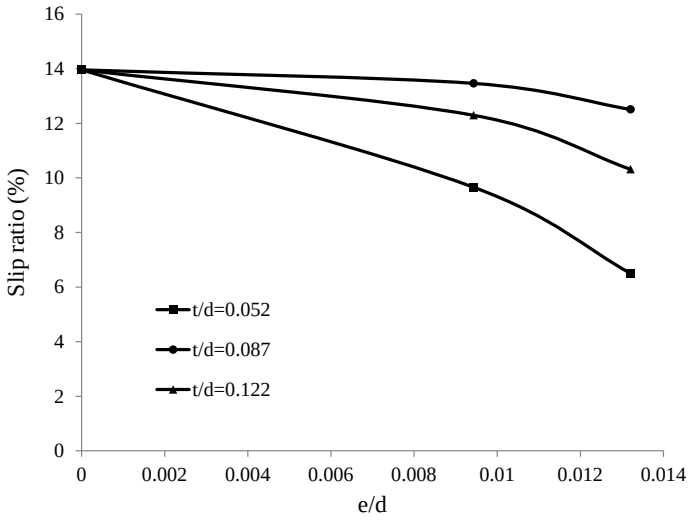

Fig. 9. *Slip ratio of rolling laterally treaded wheel with b/d=0.5 (φ=45^o, ψ=0^o, c/γgd=0.25) versus the lateral tread ratio e/d for various lateral tread ratios t/d.*

5. Conclusions

The indentation and rolling responses of a rigid wheel in cohesive and frictional soils are presented. The effects of the aspect ratio on the quasi-static steady state response of the rolling wheel were investigated. It was found that the wheel sinkage decreases as its width increases; the same is observed for increasing dilation angle of the underlying soil. A novel approach has been presented for the matching of Mohr-Coulomb and Drucker-Prager models in three dimensions, which is confirmed by the numerical results. The bulldozing effect has been successfully reproduced during the analyses and the effects of the longitudinal and lateral tread patterns on the wheel slip ratio have been investigated. Further research regarding the rigid wheel-soil interaction could include the consideration of deformable wheel, treads in an oblique direction with respect to the axis of motion, or the inclusion of the possibility of varying velocity of the wheel (driven or towed).

Nomenclature

b	wheel width or the smaller dimension of the wheel/terrain contact patch	[m]
B_i	soil bearing capacity	[kPa]
c	soil cohesion (Mohr-Coulomb)	[Pa]
d	wheel diameter	[m]
d_{DP}	cohesion (Drucker-Prager)	[Pa]
e	tread height	[m]
E	soil modulus of elasticity	[Pa]
F_{MC}	failure surface of MC model	[Pa]
F_{DP}	failure surface of DP model	[Pa]
g	gravity constant	[m/s^2]
i_s	wheel slip ratio	[-]
j_d	shear displacement	[m]
k_c	parameter due to cohesive effects	[kN/m^{n+1}]
K_d	shear deformation modulus	[m]
k_φ	parameter due to frictional effects	[kN/m^{n+2}]
n	deformation exponent	[-]

p	vertical average contact pressure	[kPa]
Q_v	vertical load on wheel center	[N]
R	wheel radius	[m]
s	depth of sinkage	[m]
t	width of tread contact area	[m]
v_x	horizontal velocity of wheel center	[m/s]
z	depth of sinkage	[m]
β	friction angle (Drucker-Prager)	[deg]
γ	soil specific weight	[N/m^3]
θ	Angle describing the location of any point in the wheel –soil contact patch	[rad]
θ_1	angle of initial contact with soil	[rad]
θ_2	exit angle	[rad]
ρ	soil density	[kg/m^3]
σ_n	normal stress distribution	[Pa]
τ	shear stress	[Pa]
φ	soil friction angle (Mohr-Coulomb)	[rad]
φ_d	epicentral angle of lateral tread	[deg]
ψ	soil dilation angle	[deg]
ω	angular velocity of the wheel	[rad/s]

Acknowledgements

This work was supported by Jaguar Land Rover and the UK-EPSRC grant EP/K014102/1 as part of the jointly funded Programme for Simulation Innovation.

References

Ageikin, J., 1981. Off-the-road mobility of automobiles. New Delhi: Amerind Pub.Co

Bekakos, C.A., Mavros, G., Prins, J. 2014. Analytical and finite-element study of the role of tread void ratio in terramechanics tyre behaviour. Proceedings of the 4th International Tyre Colloquium, 313–322.

Bekker, M. G., 1956. Theory of Land Locomotion. The University of Michigan Press, Ann Arbor.

Chiroux, R. C., Foster, W. A., Johnson, C. E., Shoop, S. A., Raper, R. L., 2005. Three-dimensional finite element analysis of soil interaction with a rigid wheel. Applied Mathematics and Computation, 162(2), 707–722.

De Borst, R., Vermeer, P.A., 1984. Possibilites and Limitations of Finite Elements for Limit Analysis Geotechnique, Vol. 34, No.2, 199-210

Hambleton, J. P., Drescher, A., 2008. Modeling wheel-induced rutting in soils: Indentation. Journal of Terramechanics, 45(6), 201–211.

Hambleton, J. P., Drescher, A., 2009. Modeling wheel-induced rutting in soils: Rolling. Journal of Terramechanics, 46(2), 35–47.

Janosi, Z., Hanamoto, B., 1961. The analytical determination of drawbar pull as a function of slip for tracked vehicles in deformable soils. Proceeding of the 1st International Conference on the Mechanics of Soil-Vehicle Systems, Torino, Italy.

Lyasko, M., 2010. LSA model for sinkage predictions. Journal of Terramechanics, 47(1), 1–19.

Shoop, S. A., 2001. Finite Element Modeling of Tire-Terrain Interaction. University of Michigan, Report number: ERDC/CRREL TR-01-16

Wong, J. Y., Preston-Thomas, J., 1983. On the characterization of the shear stress-displacement relationship of terrain. Journal of Terramechanics, 19(4), 225–234.

Wong, J. Y., Reece, A. R., 1967a. Prediction of rigid wheel performance based on the analysis of soil-wheel stresses part I: Performance of driven rigid wheels. J. Terramechanics, 4 (1), 81–98.

Wong, J. Y., Reece, A. R., 1967b. Prediction of rigid wheel performance based on the analysis of soil-wheel stresses part II: Performance of towed rigid wheels. J. Terramechanics, 4 (2), 7–25.